PRE-STRESSED MODAL ANALYSIS OF A TURBINE SPACER

M. Attia, J. Hou
Air Vehicles Division, Defence Science & Technology Organisation (DSTO)
506 Lorimer St, Fishermans Bend, Victoria Australia

marco.attia@dsto.defence.gov.au; jianfu.hou@dsto.defence.gov.au

Abstract

This paper presents finite element (FE) analyses conducted in order to determine possible high cycle fatigue (HCF) failure modes causing the cracking of a turbine spacer in a gas turbine engine. During an overhaul of a turbine module, a turbine spacer was found cracked at the forward outer rim. Inspection of the spacer suggested that the cracking was caused by HCF. As the loading mechanism for initiation and the dynamic behaviour of the spacer was unknown, an investigation by means of FE analyses was undertaken; including both steady-state and vibration analysis of the spacer. The FE modelling, analysis and findings are summarised in this paper.

1 Introduction

The turbine module in a gas turbine engine experiences both centrifugal and thermal loading under normal operating conditions. During an overhaul of a turbine module, a spacer was found cracked at the forward outer rim. The DSTO conducted a forensic investigation to determine the nature of the cracking and found that the crack had been propagating under an HCF loading regime. However, no loading mechanism for initiation was able to be identified. The engine's original equipment manufacturer (OEM) was informed of the cracking and indicated that 13 other cases of cracked spacers had been reported among the operators of the same type of engine worldwide. Most of these cracked spacers were believed to have been caused by HCF, but no loading mechanism for initiation of the fatigue cracks could be established. The spacer cracking raised a serious concern as to how many aircraft powered by this engine could be susceptible to cracking.

In order to determine the loading mechanism for crack initiation of this type and the dynamic behaviour of the spacer, further investigation was undertaken by the DSTO. FE steady-state stress analysis was conducted to identify the most representative loading conditions for the spacer and then a subsequent pre-stressed modal analysis was performed to examine the possible vibration modes that correspond to the cracking mode. This paper presents the analyses conducted and findings from these analyses, as well as discussion of possible failure modes.

2 Finite Element Modelling of Turbine Spacer

2.1 Geometry and Finite Element Modelling

An initial 2D axi-symmetric FE model of the turbine assembly of the gas turbine engine was used to create a 3D sub-model of the spacer. The 2D model, as shown in Figure 1, including all of the turbine discs, blades and spacers, as well as the tie bolts, was validated under a different program. The model also included a loading history and FE results corresponding to a complete flight profile.

The turbine assembly model was used to create a 3D sub-model of the spacer; this was required in order to perform the modal analysis. A 3D FE sub-model was generated by sweeping

the 2D mesh of the spacer around the rotor axis by 360 degrees. Figure 2a shows the forward side view of the cracked turbine spacer whilst Figure 2b shows the 3D FE model.

PATRAN [1] was used for this analysis as the pre- and post-processors whilst all FE analyses were carried out using ABAQUS Standard [2].

The 3D sub-model consisted of 72 segments around the circumference. The model, as depicted in Figure 2b, contained 31104 elements (145944 nodes), consisting predominantly of 20-noded hexahedral (hex) elements along with a minimal number of 15-noded wedge elements.

2.2 Material Properties

The spacer was manufactured out of a nickel based super alloy. The density, Poisson's Ratio and temperature dependent material properties of the alloy were incorporated in the model.

2.3 Loading and Constraints

The loads and boundary conditions applied to the 3D spacer sub-model were identical to those in the assembly model under the take-off power condition as this loading condition was assumed to represent the most severe combination of temperature and rotor speeds.

These loads and boundary conditions were defined as follows:

1. an initial temperature on the whole spacer, and
2. a rotational velocity at take-off power about the rotor axis.

The temperature contour from the 2D axi-symmetric FE results, at the time increment corresponding to the take-off power operating condition, was mapped onto the 3D spacer model.

In addition, interactions between the spacer and the surrounding turbine discs, as modelled in the 2D assembly model, needed to be included in the 3D-sub model. This was implemented by applying displacement boundary conditions at the regions where the spacer was in contact with surrounding discs, as extracted from the 2D assembly model in the stressed state.

3 Steady-state FE Model Correlation and Analyses

The FE analyses consisted of two parts: (a) an initial steady-state analysis step; and (b) a pre-stressed modal analysis step. The steady-state analysis of the 3D model was performed in order to correlate the 3D stress results with the 2D stress results acting on the spacer. The 3D steady-state analysis results were then used as initial conditions for the subsequent pre-stressed modal analysis.

3.1 FE Model Correlations

The comparison of the maximum principal stress results between the 2D spacer and the 3D spacer sub-model was made to evaluate the degree of accuracy of the 3D sub-model. As shown in Figure 4a and 4b, the stress distribution of the 3D case closely matched that of the 2D case. The difference in the peak maximum principal stresses was 3.1%

3.2 Steady-State Stress Analysis

The Steady-state FE stress analysis was performed on the 3D model of spacer. This analysis simulated the static behaviour of the spacer under the take-off power condition. The schematic diagram of the spacer with labelling of the geometric features is shown in Figure 3.

The peak stress of the spacer occurs at the forward outer web radius. Previous fractographic analyses by the OEM have shown that the forward outer web of the spacer is one of the common locations where cracks are found. However, the crack observed on this particular spacer was found at the forward outer rim. The stress contour plot in Figure 4b

indicates that the stresses at the forward outer rim area of the spacer were low under the examined operating condition. Therefore, it is unlikely that the crack at the outer rim was caused by steady-state centrifugal and thermal loading under the take-off power condition.

4 Pre-stressed Modal Analysis

Since the steady-state stresses were low at the forward outer rim of the spacer, it was important to identify if this region experienced dynamic stresses during operation. To examine the dynamic behaviour of the spacer under the take-off power condition, a pre-stressed modal analysis was performed which used the stress results of the static analysis as the initial condition.

Under the take-off power condition, the spacer rotates at approximately 13820 RPM (230 Hz). As there are 12 segments of nozzle guide vanes (NGVs) with 6 vanes on each segment upstream of the spacer, the engine order (EO) excitation would be 72 (12x6). The possible excitation frequency due to EO excitation is 72 multiplied by the rotor rotating speed (i.e. 16,584 Hz). Therefore, the possible loading mechanism may be the 72^{nd} EO excitation in the engine and frequencies up to 16,584 Hz are examined to see if there are vibration modes with high dynamic stresses at the region where the crack was found on the spacer.

The modal analysis was conducted using the Subspace iteration method and the first 99 modes were extracted. Note that for many of the natural frequencies two identical mode shapes were extracted; these modes are repeated but are offset by an integer fraction of a rotation in phase. This is a typical phenomenon that occurs for cyclic symmetric rotors.

Figure 5 shows the relative stress distributions corresponding to the first twenty vibration modal shapes. The majority of these modes showed low dynamic stresses acting on the forward outer rim. Mode 1 showed high stresses at the inner radius of the spacer at the mounting bore step. The majority of the modes (2-10 & 13-14) have high stresses occurring at the forward outer web radius. These results support why this region may be a common location where cracks can be formed if excitation sources are present. Modes 15-20, when excited, cause the spacer to experience high stresses at the aft inner web radius.

Modes 11 and 12, however, were found with high dynamic stress levels in the forward outer rim region. The stresses at these locations were not the peak stresses, however they were relatively high (70% of peak stress for these particular modes). It is possible that these modes could contribute to crack initiation at the forward outer rim location.

The remaining modes were examined and it was found that all had peak stresses at various locations around the spacer other than at the failure location. However, there were modes similar to modes 11 and 12 which resulted in high dynamic stresses at the forward outer rim region where the cracks were discovered; these modes are listed in Table 1. This table outlines the percentage stress at the forward outer rim relative to the peak stress acting on the spacer at each particular mode. The stress percentages outlined in Table 1 give an indication of how high the stresses acting at the region of interest actually are when compared to the peak stress at each mode.

The selected lower frequency modes outlined in Table 1 may be excited during engine start-up and shut-down and therefore might contribute to the crack initiation at the forward outer rim. However, these modes are unlikely to be the primary modes causing crack initiation as they are only excited over a very small period of time during engine start-up and shut-down. Modes 88 and 89 on the other hand are excited at frequencies close to the engine order excitation frequency of 16,584 Hz. These two modes, as depicted in Figure 6 are therefore likely to be excited at the engine's normal operating speed and therefore become a more likely cause of crack initiation.

Modes 90-99 did not appear to have high stresses at the forward outer rim region. These modes also occurred at frequencies higher than the engine order excitation at which the engine operates and therefore are unlikely to be the cause of any damage caused to the spacer.

5 Discussions

It should be noted that there are limitations in these FE analyses.

Firstly, it was assumed that since the steady-state take-off power condition represented the worst combination of temperature and rotor speeds, the modal analysis of the spacer under these conditions would produce the worst case scenario of dynamic stresses; this may not necessarily be the case.

Secondly, the 3D model of the spacer did not include the scallops at the forward arm which are present in the spacer; the reason being that the 3D model of the spacer was created by sweeping the 2D mesh about an axis of rotation. This may have a slight impact on the stress results in this analysis. There were small indications of wear observed on the forward outer rim on either side of the cracked scallop. As these wear marks may be somehow related to the formation of the crack at that particular scallop, further analysis may be required to incorporate the presence of the scallops.

6 Conclusion

This investigation has focused predominantly on identifying the loading mechanism leading to crack initiation at the forward outer rim, as found on a gas turbine rotor spacer. A 3D FE sub-model of the spacer was created based on a 2D (axi-symmetric) assembly model of the turbine section. Steady-state stress and modal analyses were conducted on a 3D spacer model in order to examine the behaviour of the spacer under the take-off power condition, as this condition represented the worst combination of temperature and rotor speeds.

The following conclusions can be drawn from this investigation:

1. Stress results from the 3D sub-model of the spacer showed satisfactory agreement with that from the 2D axi-symmetric analysis, confirming that the peak stresses on the spacer occur at the forward outer web radius. The forward outer rim area was found to be under low stress at the operating condition considered.
2. The loading mechanism for cracking was identified to be the 72nd engine order excitation at 16,584 Hz.
3. Pre-stressed modal analysis was performed and vibration modes were examined for frequencies up to 16,584 Hz. The results suggest that some low frequency modes may contribute to crack initiation at the forward outer rim during engine start-up and shut-down. However, these modes are unlikely to be the primary modes causing crack initiation since the excitation only occurs over a very short period. The two modes at 16080Hz are more likely to cause crack initiation because their excitation frequencies are very close to the engine order excitation frequency.

7 Recommendations

It is recommended that vibration modes under other operating conditions be examined in order to determine if other crack failure modes are excited during engine operation. It could also be beneficial to include the presence of scallops at the forward rim for a more complete stress analysis.

References

[1] *MSC/PATRAN User's Manual*. Version 2008 r1.
[2] Hibbitt, Karlsson and Sorensen Inc. '*ABAQUS User's Manual*', Ver. 6.6 2006.

Copyright Statement

8 Figures and Tables

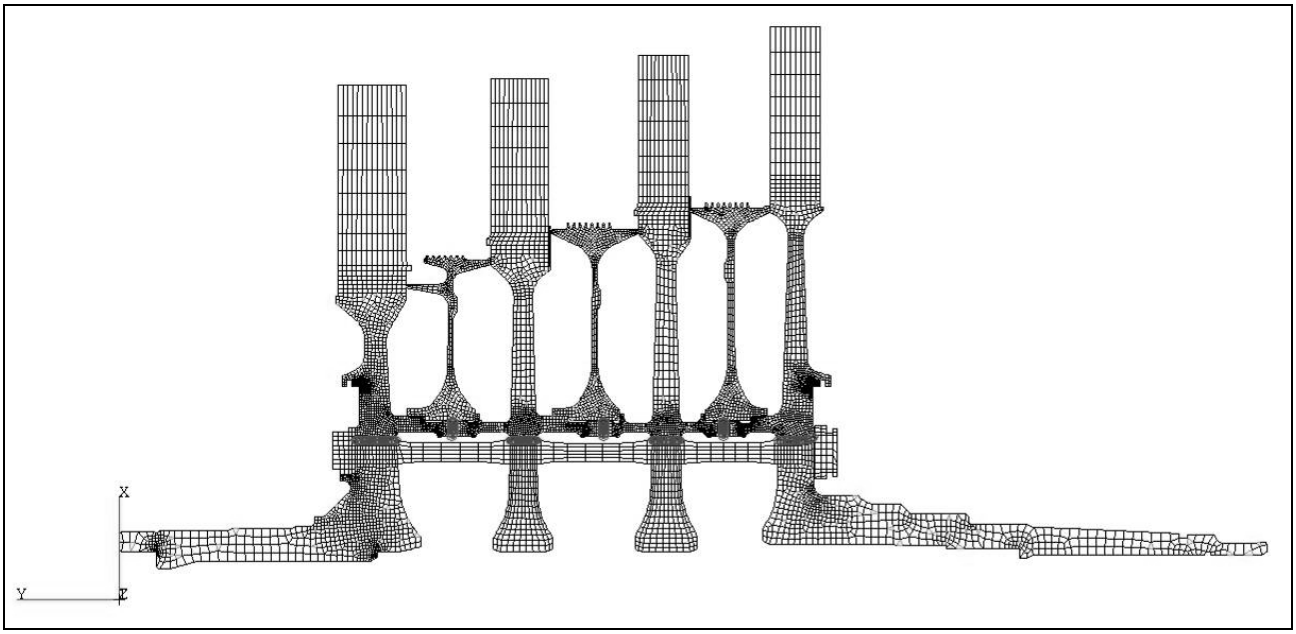

Fig. 1. 2D axi-symmetric FE model of the turbine assembly.

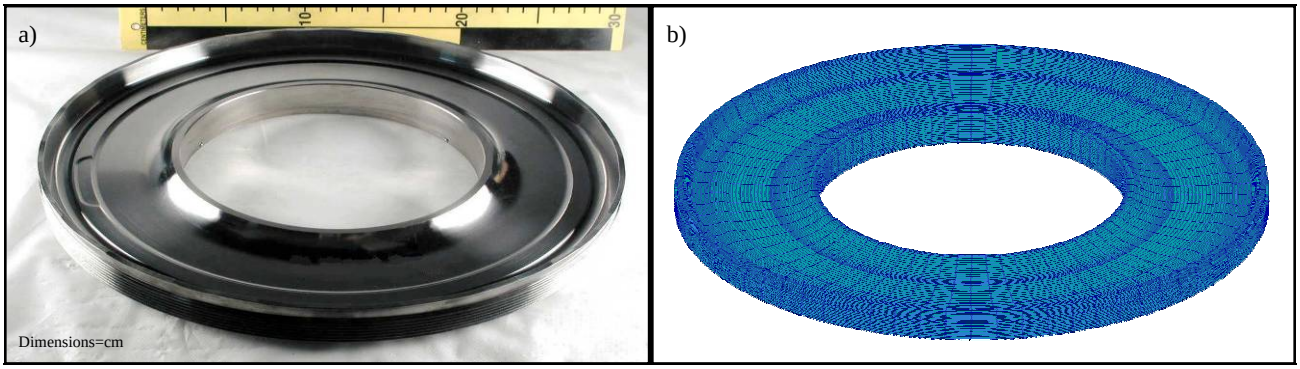

Fig. 2. Forward side view of a) the cracked turbine spacer and b) the 3D FE model.

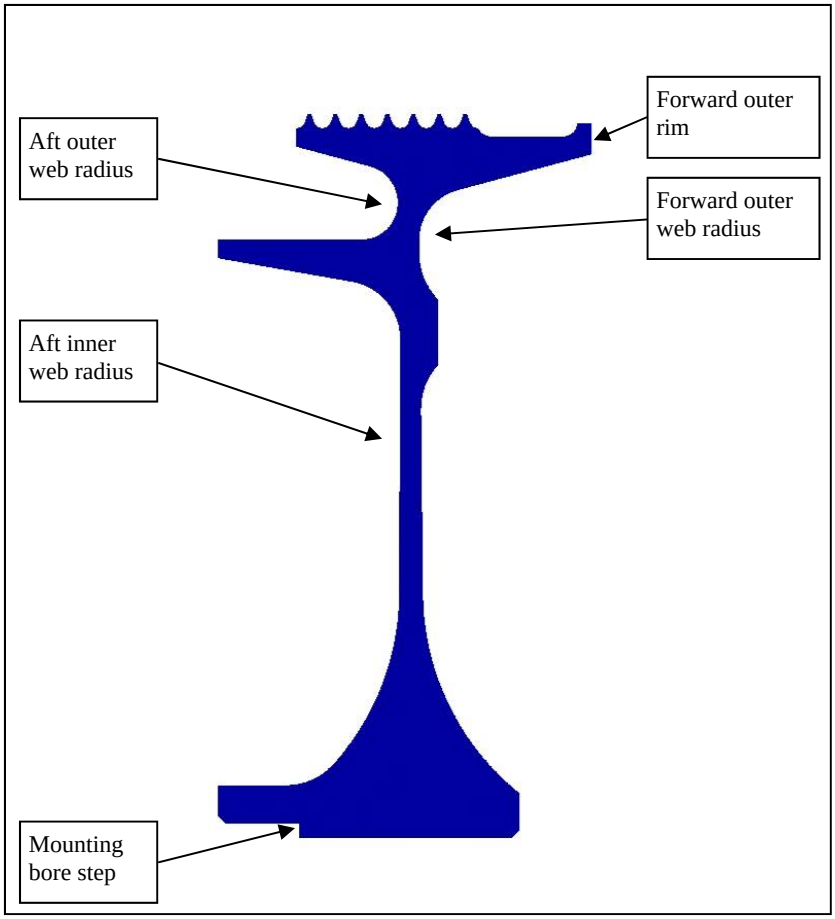

Fig. 3. Schematic diagram with labelling of the special features of the spacer.

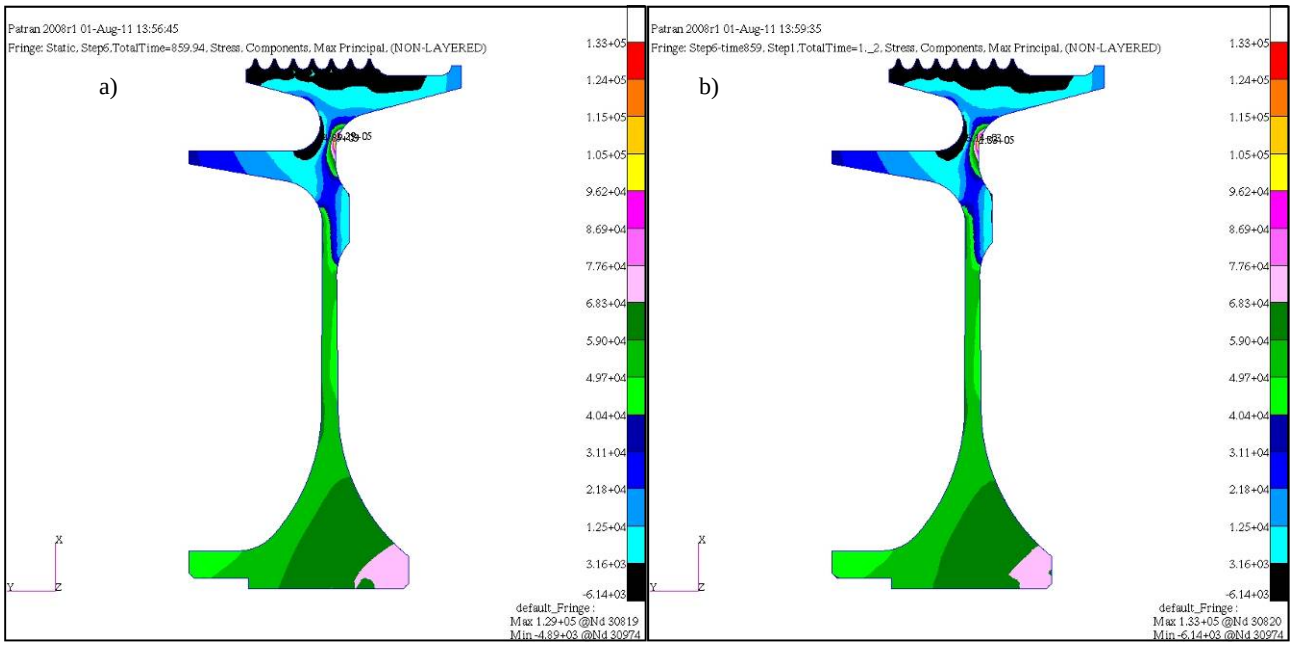

Fig. 4. Comparison of the maximum principal stress results between a) the 2D spacer (from the assembly model) and b) the 3D spacer sub-model (cross-sectional view).

Mode No.	Predicted Frequency (Hz)	Mode No.	Predicted Frequency (Hz)
1	4277	11,12	6662
2,3	4881	13,14	6939
4	5183	15,16	7710
5,6	5201	17,18	8506
7,8	5643	19,20	9306
9,10	6234		

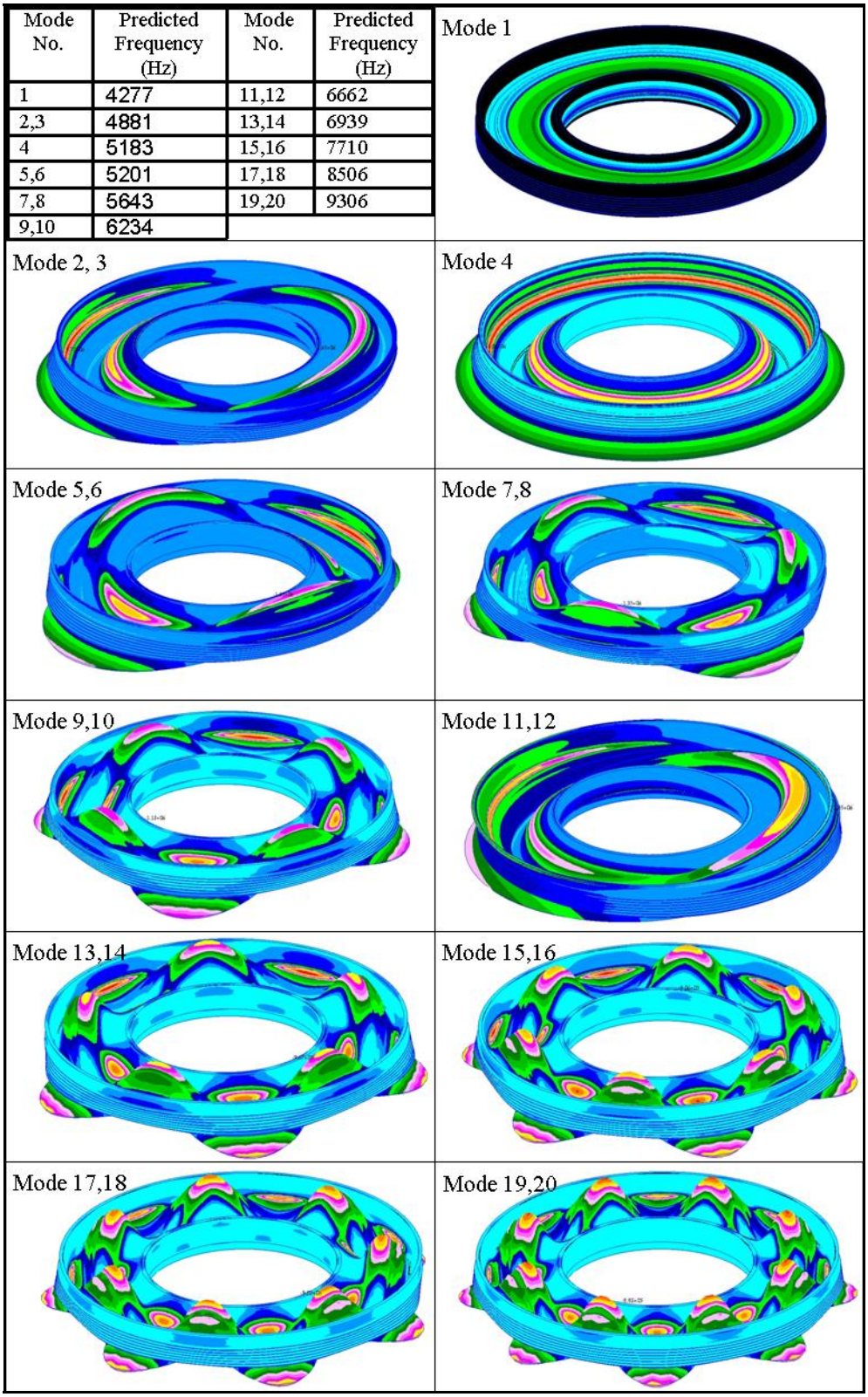

Fig. 5. Maximum principal stress distributions for the first twenty vibration modal shapes of the spacer.

Tab. 1. Modal shapes causing high stresses at the forward outer rim region.

Mode No.	Freq (Hz)	% Stress at forward outer rim to peak stress
11	6662.3	70%
12	6662.3	70%
21	9392.4	60%
22	9392.5	60%
71	15168	74%
72	15168	74%
73	15323	66%
74	15323	66%
75	15348	70%
76	15348	70%
79	15395	70%
80	15504	68%
81	15504	68%
88	16080	59%
89	16080	59%

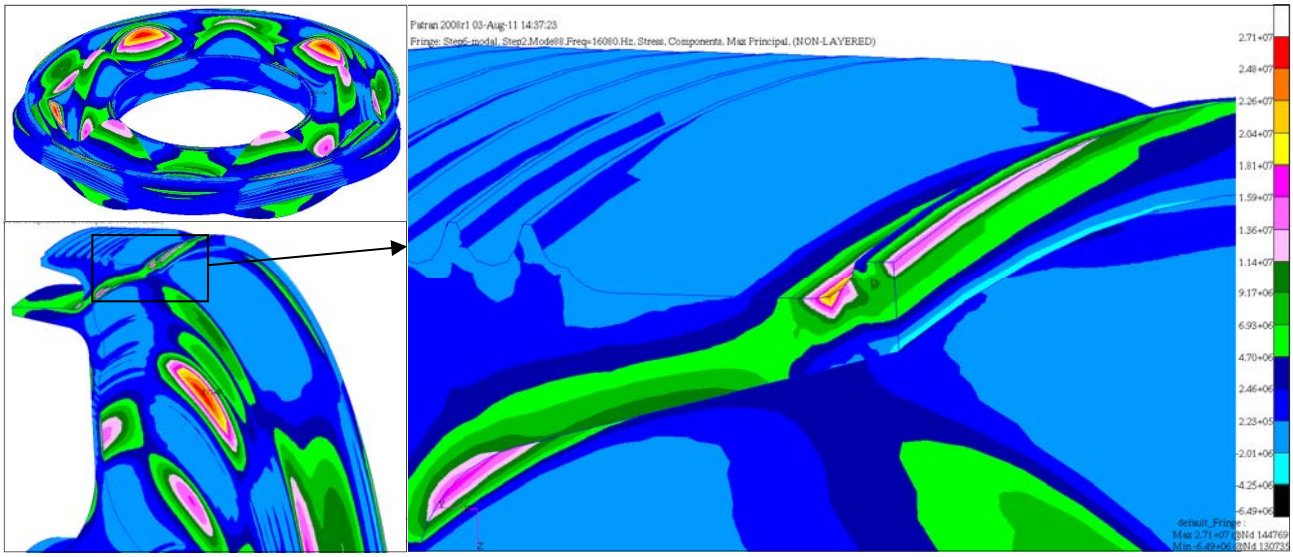

Fig. 6. Max principal stress distributions corresponding to vibration modal shapes 88 & 89.